The 6th International Supercritical CO_2 Power Cycles Symposium
March 27 - 29, 2018, Pittsburgh, Pennsylvania

Modeling and Testing of a Directly Heated Supercritical CO_2 Combustor

A.S.M. Arifur Chowdhury
Doctoral Research Assistant
Center for Space Exploration and Technology Research
The University of Texas at El Paso
El Paso, Texas, USA

Jad Aboud
Doctoral Research Assistant
Center for Space Exploration and Technology Research
The University of Texas at El Paso
El Paso, Texas, USA

Ahsan Choudhuri
Professor
Center for Space Exploration and Technology Research
The University of Texas at El Paso
El Paso, Texas, USA

Norman Love
Associate Professor
Center for Space Exploration and Technology Research
The University of Texas at El Paso
El Paso, Texas, USA

Bhupesh Dhungel
Air Liquide R&D
Delaware Research and Technology Center
Newark, Delaware, USA

Jiefu Ma
Air Liquide R&D
Delaware Research and Technology Center
Newark, Delaware, USA

Hwanho Kim
Air Liquide R&D
Delaware Research and Technology Center
Newark, Delaware, USA

Remi Tsiava
Air Liquide R&D
Paris-Saclay Research Center
Jouy-en-Josas, France

ABSTRACT

Directly Heated Supercritical Carbon Dioxide (DH-SCO_2) power cycles have the potential to achieve high thermal efficiencies and provide options for more than 90% CO_2 capture. Recent thermodynamic analysis of the DH-SCO_2 cycle performed by several groups including the UTEP-Air Liquide research team show that combustion conditions in the vicinity of 300 bar pressure and 1000-1400 K temperature allows for relatively high system efficiencies while operating within the limit of practical combustor materials. However, the realization of DH-SCO_2 cycle requires combustion systems be designed to operate in supercritical conditions and at temperatures far below the blowout limit of conventional flames (above 1500 K), where not only the thermodynamic properties but also the combustion properties and kinetics are not well known. To close this gap in data, some intermediate pressures are explored experimentally and combustor behaviors modeled for the higher pressures in this study.

For modeling of the system, a commercial computational fluid dynamics simulation tool, ANSYS Fluent, is used. The inlet conditions for the CFD analysis are obtained from the experimental study. The geometry used for the study is the same as the experimental facility and operate at the same power ratings. A comparison between experimental and modeling results are presented in this paper. The knowledge obtained from this study is essential to accurately and safely design combustors for supercritical conditions.

For the experimental portion of this study, an oxy-fuel high-pressure combustor, designed to operate at up to a 250kW power input and 20bar pressure, is used operating with oxygen and methane. This is a systematic first step in testing at supercritical conditions. The combustor is fitted with an internal cooling ring that has the ability to inject CO_2, shielding the combustor wall from the high oxy-combustion temperatures. This cooling system is not used in the current system but is included in the paper. A shear-coaxial injector is used to mix the fuel and oxidizer and two high pressure igniters are used for system start-up. The combustor is lined with pressure and temperature sensors and controlled via LabView. For this paper experimental results are presented for pressures of 7 bar (case 1) and 16 bar (case 2). However, the CFD simulation is presented for only case 1. The data obtained from 7 bar pressure experiments are used for validation and verification of the CFD models. It is found from the analysis that detailed chemistry must be incorporated with the CFD simulation to accurately predict the combustion characteristics at high pressure.

NOMENCLATURE

d_i	=	High velocity jet diameter	(m)
$\dot{m}_{methane}$	=	Methane mass flowrate	(kg/s)
$\dot{m}_{oxygen}$	=	Oxygen mass flowrate	(kg/s)
$\dot{m}$	=	Exhaust mass flowrate	(kg/s)
F.I.	=	Firing input	(W)
LHV	=	Lower heating value	(kJ/kg)
v	=	Velocity	(m/s)
VR	=	Velocity ratio	(-)
J	=	Momentum flux ratio	(-)
$v_{methane}$	=	Methane velocity	(m/s)
v_{oxygen}	=	Oxygen velocity	(m/s)
A	=	Exit Area	(m^2)
P_t	=	Total pressure	(Pa)
P^*	=	Exit pressure	(Pa)

P_0	=	Chamber Pressure	(Pa)
T_t	=	Total temperature	(K)
R	=	Gas Constant	(J/kg-K)

Greek

ρ	=	Density	(kg/m^3)
γ	=	Specific heat ratio	(-)

INTRODUCTION

Oxy-fuel combustion refers to burning a hydrocarbon with oxygen resulting in an exhaust stream which is comprised mainly of carbon dioxide and water vapor[1-3]. The benefits of this system are that higher temperatures theoretically permit higher achievable efficiencies, the exhaust products are free of NOx, thereby allowing for capture of as high as 100 % carbon dioxide at the post-combustion stage [2- 6]. Since carbon dioxide produced in the exhaust stream is high purity, minimal processing is required, permitting for less energy intensive carbon capture. In addition, oxy-combustion provides similar or higher efficiencies compared to air fired systems despite additional parasitic loads of the air separation and carbon capture units[7].

In the last several decades, high pressure combustion applications have been investigated extensively. Carroni et al.[8], Tse et al.[9], Singla et al[10] have been successfully conducting experiments on high pressure/trans-critical combustion accommodating air-methane, oxy-methane and LOx-H_2 in different pressure environments. Carroni et al[8] conducted high pressure experiments and have modeled air-methane catalytic combustion for power generation applications. Tse et al[9] designed and built an optically accessible high-pressure combustion apparatus to observe the morphology and development of premixed reaction fronts at elevated pressure. The authors followed a chamber-in-chamber design approach to manufacture the combustor for constant pressure combustion experiments. Singla et al.[10] have studied the transcritical oxygen/transcritical or supercritical methane combustion. For the most part, in liquid propellant engines the reactants are injected at subcritical temperature into an environment in which the temperature and pressure exceed the thermodynamic critical conditions. In this experimental study, a similar concept has been used to conduct high pressure oxy-fuel combustion testing. The combustion chamber pressure has been kept between 4.5 to 6 MPa (45 bar to 60 bar) while the reactants are initially in subcritical stage. The study has been conducted for methane, hydrogen and nitrogen flames. All these concentrated studies are conducted to characterize combustion parameters and fluid behavior in a high pressure environment.

Motivated by the advantages of oxy-combustion, the purpose of the experimental portion of the study is to develop a high pressure (< 20 bar) oxy-methane combustor and produce data needed to validate models for supercritical conditions. The combustor for the experiment was previously developed by Sarker et al[12]. The combustor designed by Sarker et al[12] operated on air as the oxidizer and required modifications in order to operate on oxygen instead. To perform the high-pressure combustion experimentation, a burner is developed and the combustor is modified to accommodate the oxy-methane combustion temperature requirements. In this paper, the design approach is presented and experimental methodologies shown for the methane-oxygen burner, ignition system, and the flow delivery systems.

A 2D computational fluid dynamics (CFD) analysis is also performed as part of this work using

the same geometric and fluid flow boundary conditions as the experiment. Afterwards, a quantitative and qualitative comparison is conducted between the CFD analysis and the test data.

DESIGN METHODOLOGY

The design methodology of a methane-oxygen burner, igniter, and end cap are discussed in this section. A shear coaxial injector is used for the burner. The shear-coaxial injector utilizes the shear between the fuel and oxidizer to mix the two streams[13-18]. The shear forces are driven by the momentum flux difference between two streams. A previously used rocket thruster is used as the igniter[19]. Initially a CFD analysis is conducted on this burner at the expected experimental test conditions to model the flame length, flame temperature and near wall temperature profile. Based on the CFD analysis several modifications were made to the combustor to adjust the ability of the system to accommodate oxy-combustion, instead of air-based burning.

A. Burner Design

For this experimental study, the shear co-axial injector is designed to operate at a firing input of up to 250 kW and 20 bar pressure. Methane is used as the fuel along with pure oxygen as the oxidizer. The oxygen port is designed in such a way that carbon dioxide can added as a diluent if required; however, is not used in the present study. The mass flowrate for the methane and oxygen are calculated from the power input using Eqs (1) and (2) at stoichiometric conditions. The lower heating value (LHV) characterizes the heat of combustion of the fuel. The lower heating value of methane is 50,000 kJ/kg. At stoichiometric conditions the $^{O}/_{F}$ ratio is 4.

$$\dot{m}_{methane}=\frac{\text{Firing Input}}{\text{LHV}} \tag{1}$$

$$\dot{m}_{oxygen} = \dot{m}_{methane} \times \left(^{O}/_{F}\right)_{st.} \tag{2}$$

When designing the shear-coaxial injector, two non-dimensional parameters re used, velocity ratio (VR) and momentum flux ratio (J). The formula for velocity ratio and momentum flux ratio are shown Eqs (3) and (4)[13].

$$VR = \frac{v_{methane}}{v_{oxygen}} \tag{3}$$

$$J=\frac{(\rho.v^2)_{methane}}{(\rho.v^2)_{oxygen}} \tag{4}$$

For this particular study, the burner and velocity ratios are varied between 4.85 to 7, momentum flux ratios are varied between 12 to 20. Lux et al[19] uses similar ranges of velocity ratios and momentum flux ratios to design a high-pressure liquid oxygen/methane coaxial injector. The image of the burner can be seen in Fig. 1. The maximum operating conditions for the burner can be found in Table 1.

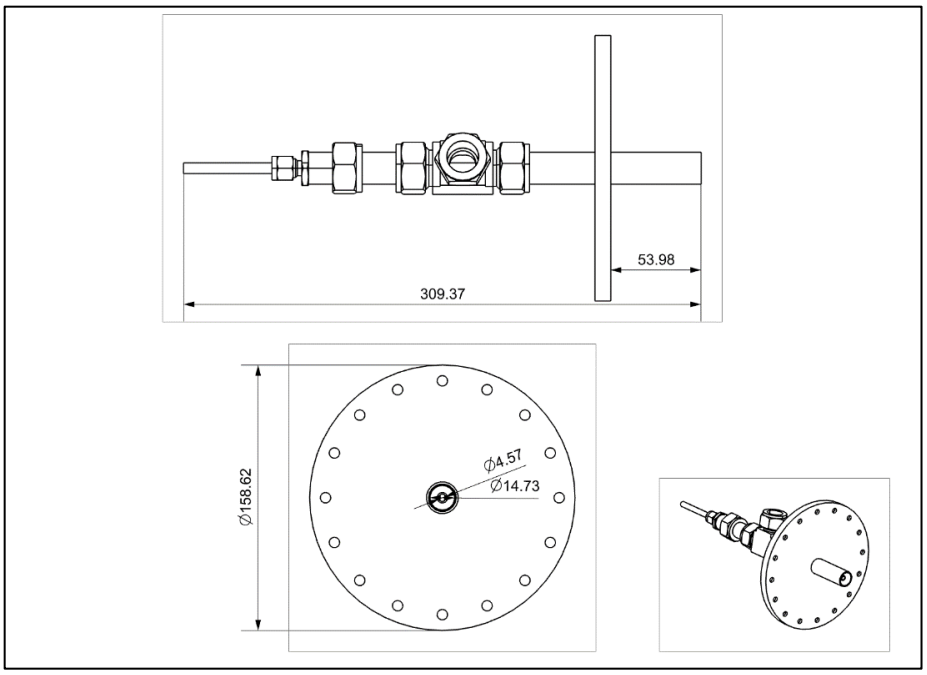

Figure 1. Main burner, units in mm

Table 1. Main burner operational limits

Power Input (kW)	250
Operating Pressure (bar)	20
Momentum flux ratio	2-20

Previous studies have shown that by recessing the high velocity jet port with respect to the injection plane, combustion performance is enhanced[13]. Kendrick et al[16] found that a recess of $1d_i$ (where d_i represents high velocity jet diameter) in LOx/H_2 combustion, increases the flame expansion rate and width of the flame volume. Tripathi et al[17] investigated the effect of momentum flux ratio on recess length. The authors found that the effect of recess length is higher when the momentum flux ratio is small. However, it is demonstrated that increasing the recess length above $1.5d_i$ does not improve the combustion performance[17]. Wheeler and Kirby[18] found that a recess length close to $1.3d_i$ in LOx/CH_4 combustion demonstrates enhancement in terms of combustion efficiency. For the proposed injector, the recess length of $1d_i$ is used, Fig. 2.

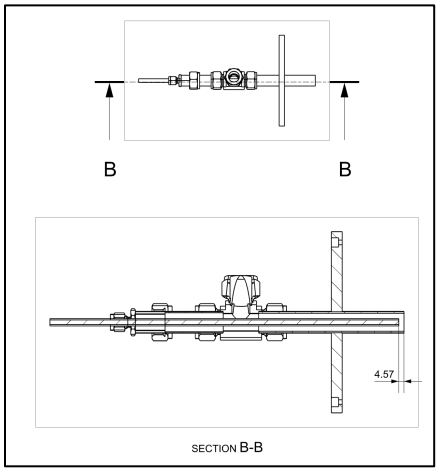

Figure 2. Main burner methane port recess length, units in mm

B. Igniter Design

The main burner is ignited using a pilot flame. The pilot flame inlets are situated at the two sides of the combustor. The igniter design is modified from Sanchez et al[19]. The igniter is designed to operate using oxygen and methane. The ignition system uses an internal swirl injection. The oxidizer flows through an axial inlet and is surrounded by four tangential fuel inlets that create a swirl that mixes with the oxidizer prior to ignition. The igniter can be seen in Fig. 3. The inlet connections for the igniter burner fuel and oxidizer are 1/4-inches (6.35 mm) and 3/8-inches (9.525 mm) tubing, respectively. The inlet pressures of the fuel and oxidizer range in pressure from 8 to 13 bar. The unit is fitted with D series Cryogen Solenoid valves connected with 1/4-inch (6.35 mm) tubing. These valves have a maximum operating pressure of 25 bar. The igniter is designed to be installed onto a 0.532-inch (13.5 mm) diameter hole so that the flame exit is flush with the combustion device inner wall. A circular boss is fabricated with a matching thickness to install the 1.5-inches (38 mm) long tube of the igniter into the combustion device. It is necessary to close the igniter inlet valves when the combustion chamber pressure exceeds the inlet pressure to the igniter valve to prevent back flow into the igniter. The igniter continuous operational burn time is 3 to 5s. The operating conditions for the igniter can be found in Table 2.

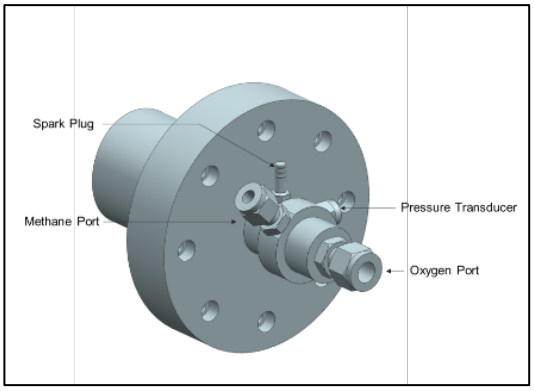

Figure 3. Igniter

Table 2. Igniter operating conditions

Inlet Igniter Port Pressures (bar)	8 – 13
Combustion Chamber Pressure (bar)	5- 10
Mixture Ratio	1-3
Maximum burn time (s)	5

A standard 1/4-32 spark plug (PART #: EVOG10350) is the ignition source for the igniter. The voltage output of the spark plug when connected to a 5V 2.4A power source with a signal generation is 12kV.

C. End Cap Design

The existing combustor has an exit inner diameter of 280 mm. However, to pressurize the combustor up to 20 bar the exit area must be reduced. The combustor is pressurized by manipulating the exit area. For this purpose, the exit of the combustor is restricted using a converging nozzle. For ideal conditions, the critical pressure ratio for hot combustion gas products is 0.58[20]. The critical pressure ratio can be calculated from Eq. (9)[20]:

$$\text{Critical Pressure Ratio} = \frac{P^*}{P_0} \tag{9}$$

Where, P* is the exit pressure and P_o is the chamber pressure. During the test, the combustion products are released into the atmosphere (1 bar). For this case, the maximum chamber pressure is 20. Thus, the exhaust is choked at the exit for a given nozzle exit area. The throat area is calculated using Eq. (10)[20].

$$\dot{m} = \frac{A*P_t}{\sqrt{T_t}}\sqrt{\left(\frac{\gamma}{R}\right)\left(\frac{\gamma+1}{2}\right)^{\frac{-\gamma+1}{2(\gamma-1)}}} \tag{10}$$

Based on these design parameters, the combustor end cap is designed to achieve choked flow at the exit. The combustor end cap consists of three flanges. The first flange is attached with the combustor main body and the second flange is bolted onto the first flange. The diameter reduction from the first and second flanges are 178 mm and 76 mm, respectively. The third flange is attached with the second flange. The third flange is equipped to attach a small exit diameter adapter to pressurize the combustor, Fig. 4.

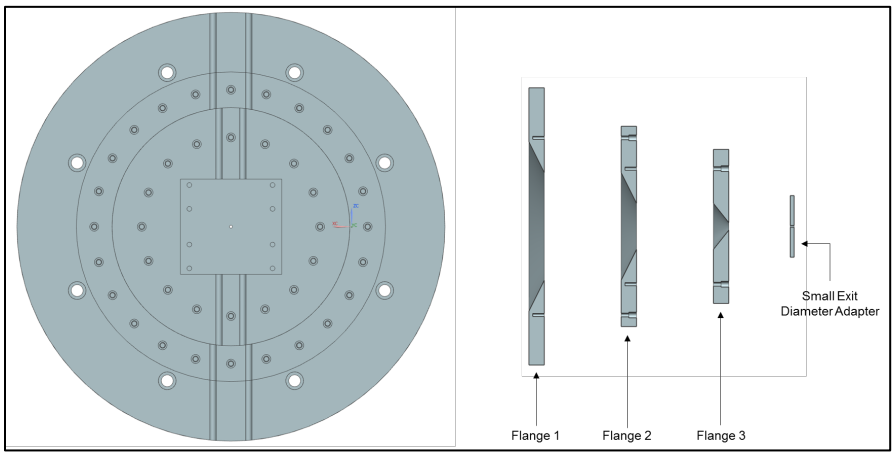

Figure 4. Combustor end cap

EXPERIMENTAL METHODOLOGY

The experimental apparatus consists of three main components: (I) feed system, (II) the data acquisition and control system and (III) the combustor. The feed system is remotely controlled using a data acquisition (DAQ) system. The combustor is mobile and positioned on a trailer. These mobile facilities allow for the transporting of the test setup to a remote location during a test day for safety. For this reason, the DAQ system is also transportable. The following sections provide more details on the initial experimental test system.

A. Feed System

The feed system consists of a bank of gas tanks fitted with tank regulators, needle valves, solenoid valves, manual ball valves, thermocouples, pressure transducers and flowmeters. The fuel, oxidizer, and diluents are delivered from K-bottles. The K-bottles are situated in two different locations. The K-bottles for the main burner are located 15 m away from the combustor. Additional K-bottles are also for the igniters are located adjacent to the combustor. The detailed view of the feed system can be found in Fig. 5. The area bounded by the red rectangle is located 15 m away from the main test side. This is where the main burner gas tanks are situated. The gas tank regulators are selected based on the test conditions. The maximum operating pressure during the test is 20 bar. Therefore, the tank regulators are selected to provide up to a 35 bar delivery pressure. The needle valves are positioned right after the regulators. This facilitates controlling the gas flow during the test if necessary. During the test, carbon dioxide is used as the diluent. A thermocouple is placed in the diluents line. The carbon dioxide possesses the threat of condensation during the expansion process and thus was not used. Nevertheless, a thermocouple in the line measures the fluid temperature. The normally closed solenoid valves are put in the line to remotely control the flow. The solenoid valves have a response time of 0.5 s for opening the valves. The manual ball valves are placed to control the gas flow and isolate different

system sections. The abundance of manual ball valves and solenoid valves enhance system compartmentalization and safety. These valves also provide enhanced control during the operation of the system.

The methane and oxygen tank regulators have 1/4” (6.35 mm) compression outlet connections. The carbon dioxide tank regulator has 1/2” (12.7 mm) compression outlet connections. The 15 m tubing between the main burner methane, oxygen, carbon dioxide gas tanks and the trailer valve train is 1” (25.4 mm) tubing. An adapter is used to convert the 1/4” (6.35 mm) and 1/2” (12.7 mm) tubing to 1” (25.4 mm) tubing. Afterwards, different sizes adapters are used to feed fuel, oxidizer and diluents into the combustor. The inlet connections for the main burner fuel is 1/4” (6.35 mm) and oxidizer connection is 3/4” (19.05 mm) tubing. The inlet connections for the igniter, and burner fuel and oxidizer ports is 1/4” (6.35 mm) and 3/8” (9.53 mm) tubing, respectively. The cooling manifold has eight inlets. The inlet connections for the cooling system manifolds are 1/2" (12.7 mm). The feed lines are leak checked using nitrogen gas. Photographs of the feed system can be seen in Fig. 6.

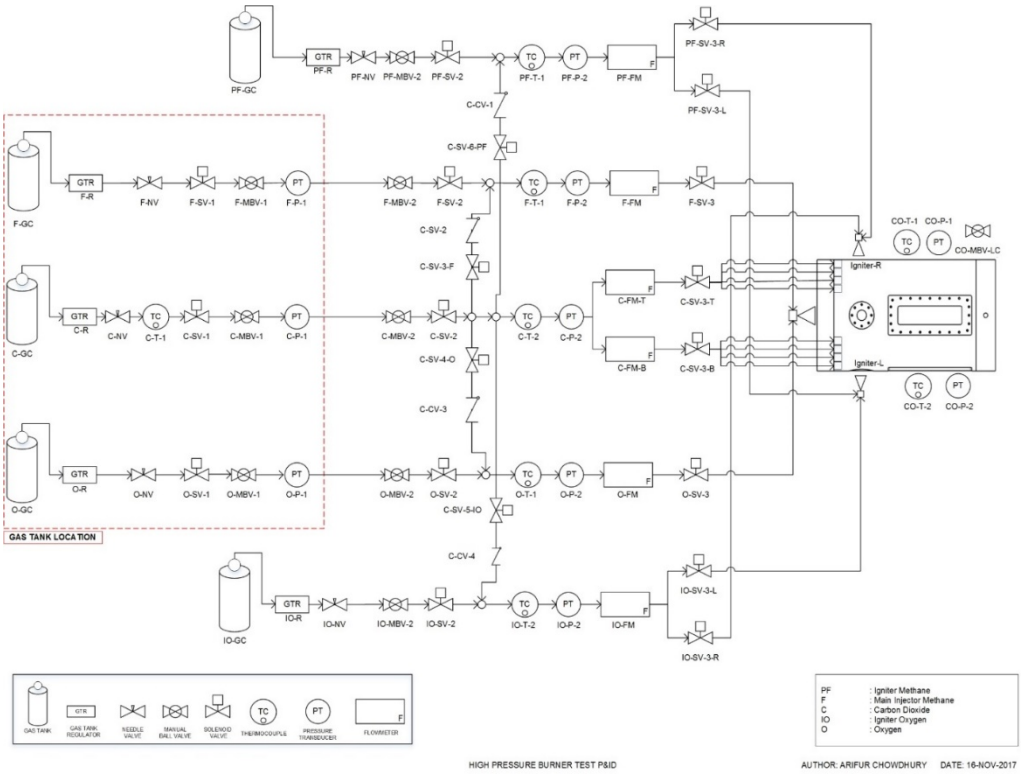

Figure 5. System piping and instrumentation diagram

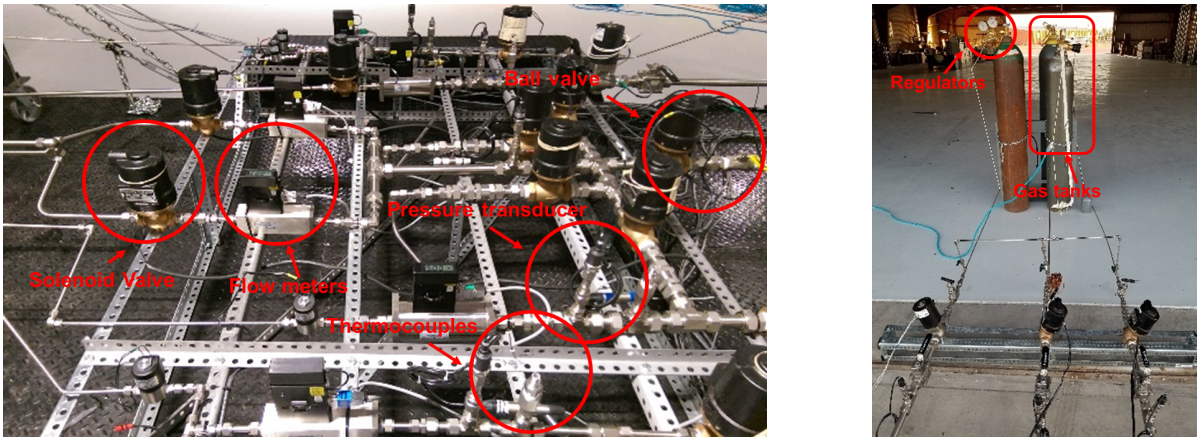

(a) (b)

Figure 6. (a) Valve train on the trailer (b) K-bottles located 15m from the test site

B. Data Acquisition and Control System

The data acquisition and control system provides remote access to the valve train. The solenoid valves are remotely operated using the DAQ. The thermocouples, pressure transducers and flowmeters also feed data into the system. The schematic for the DAQ system can be seen in Fig. 7. The main test setup to the DAQ station provides supervisory, control and data acquisition signals for both direct and alternating current devices on the burner test and the burner test feed system. The test station houses an Ethernet network allowing DAQ systems to communicate to a remote computer or data center via fiber-optic link. The test station and all instrumentation power is provided by the test station via a three phase 120 VAC/60Hz grounded power source. The test station has the capacity of controlling up to 64 solenoids and recording data from 32 pressure transducers, 32 flowmeters, and 60 thermocouples.

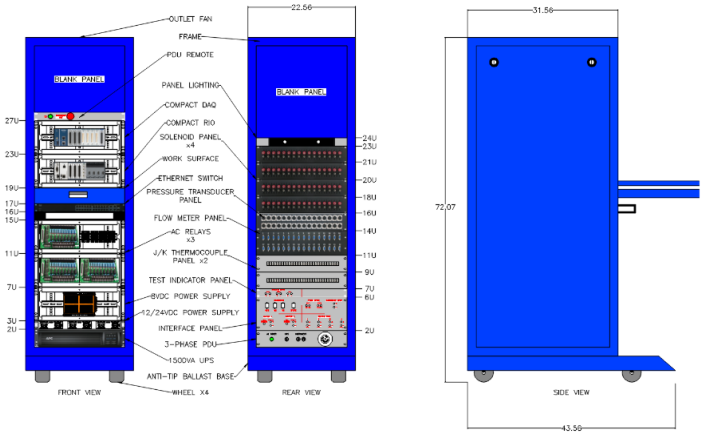

Figure 7. DAQ system schematic

The LabVIEW control interface can be found in Fig. 8. The LabVIEW window provides real time information about the line pressure, line temperature, flowrates, combustor pressure and combustor temperature. During the test, at the beginning the lines are pressurized by manually opening the solenoid valves. The combustor is equipped with two different igniters. Two of these igniters have separate spark plugs. The spark plugs can be operated using the program. The LabVIEW is programmed such a way that the test can be conducted using pre-programmed auto sequence. It also allows to record the necessary data during the test. It is also equipped with 'EMERGENCY STOP'. The 'EMERGENCY STOP' can be initiated due to any malfunctioning

during the test. The ‘EMERGENCY STOP’ will also be automatically initiated if the combustor wall temperature reaches above 600K or feed line pressure exceeds 25 bar.

Figure 8. LabVIEW interface

C. Combustor Test Bed

The combustor is placed on a 6 m x 2 m trailer. The combustor stand is secured with the trailer using three metal chains. The igniter fuel and oxidizer gas tanks are also positioned on the trailer. The gas tanks are strapped with the tank stand. The tank stand is bolted onto the trailer. The trailer rests on four mechanical jacks. Two of the jacks can carry 6 metric-tons of weight and the other two jacks can carry 4 metric-tons. During the test, the trailer is transported outside the facility building and placed 15 m away from the building.

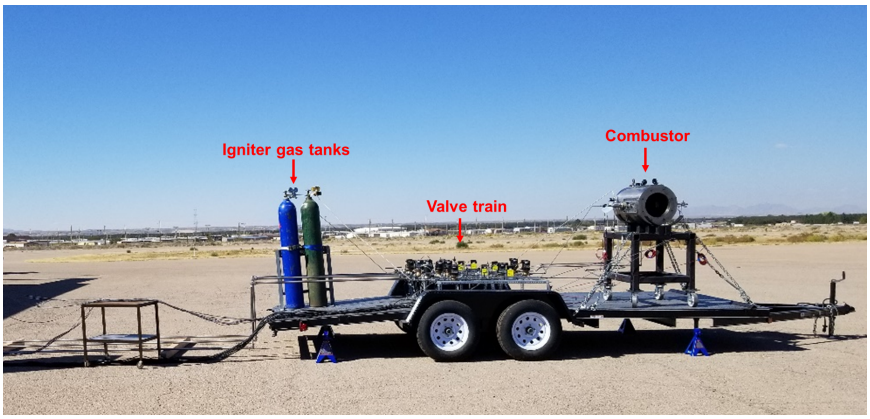

Figure 9. Combustor test setup

NUMERICAL METHODOLOGY

A numerical analysis is conducted using ANSYS Fluent. The geometry and mesh are also generated using ANSYS software. The CFD analysis is performed to replicate the test conditions. During the analysis, the input parameters are obtained from the experimental portion of the study. Then a quantitative and qualitative comparison is performed between the CFD results and the test data.

A. Geometry and Mesh

A 2D domain is used to reduce the computational time. The simplified geometry consists of the burner, igniter, and end cap. The combustor has an inner radius of 0.14 m and is 0.65 m long. While creating the 2D geometry, the dimensions are selected based on the experimental setup. The equivalent areas for the different ports used in the model are provided in Table 3:

Table 3. 2D geometry at various sections

Port Type	Cross-Sectional Area (m^2)
Main Burner (CH_4)	1.64E-05
Main Burner (O_2)	1.63E-04
Exit Diameter	1.27E-04

An additional fluid domain located outside of the exit nozzle section is also included. The pressure boundary condition is input at the end of the added fluid domain. By doing this, the simulation calculates the pressure inside the combustor based on the combustion product composition, gas temperature, and exit area.

The whole geometry is divided into three sections to achieve better control over the mesh dimensions. The total number of elements and nodes are 74,082 and 73,171, respectively.

B. Boundary Conditions

A transient density-based solver is used for the calculations. The density-based solver is selected since the flow through the nozzle at the exit of the combustor is choked. Turbulence models are used to simulate combustion inside the combustor, k- ε(standard). For the combustion, the non-premixed combustion model is employed. For simplicity, single step chemistry is used for the current model. Multistep chemistry is expected to provide more accurate results and is currently under investigation by the authors using a reduced Aramco mechanism. Results from the multistep chemistry analysis will be presented in future publications.

The DO radiation model is also incorporated to simulate the radiation effect. It is believed that the high temperatures in the oxy-flame will make radiative heat transfer significant. The WSGG (Weighted-Sum-of-Gray-Gases) domain-based method is used to calculate the absorption coefficients. The wall emissivity is set to 0.9.

A summary of the boundary conditions used in the computational model is shown in Table 4.

Table 4. Boundary conditions

Section	Input
General	
Type	Transient Density Based
Models	
Turbulence Model	Standard k- ε model
Radiation	Discrete-Ordinate model
Species	Species Transport (One Step Chemistry $CH_4+2O_2=2H_2O+CO_2$)
Turbulence-Chemistry interaction	Eddy-Dissipation model
Boundary Conditions	
Method	2D Axisymmetric
Inlets	- Pressure Inlet: Fuel (Methane) Inlet - Pressure Inlet: Oxidizer (Oxygen) Inlet
Outlet	Pressure Outlet: 1 bar
Wall	Wall: Adiabatic

RESULTS AND DISCUSSION

In Figure 10 the location of the video camera is shown with respect to the combustor. Accordingly, Figure 11 to 13 show the video screenshots from the camera for operational case 1 (7 bar). During the experiment, the main burner is ignited using the pilot flame, Fig 11. The igniter is run for 4s. During the last 2s of the igniter operation the main burner fuel and oxidizer line is opened, and the main burner is ignited (Fig 12). The main burner is then operated for 20s. Figure 13 demonstrates the ignition of the gases in the combustor.

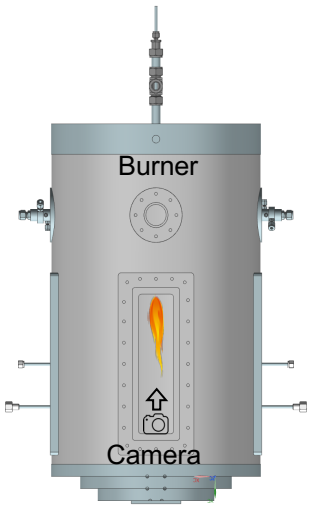

Figure 10. Camera location

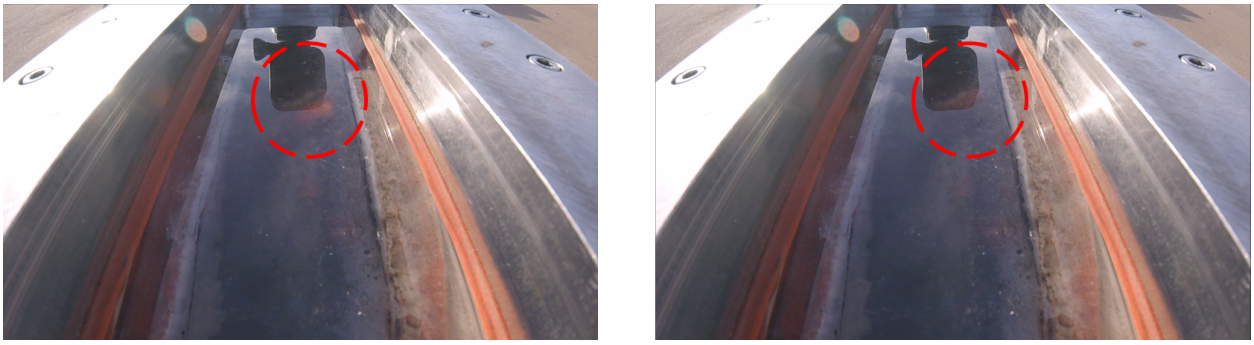

Figure 11. Screenshot from video of igniter flame at beginning of test, Case 1. The igniter flame is circled in red.

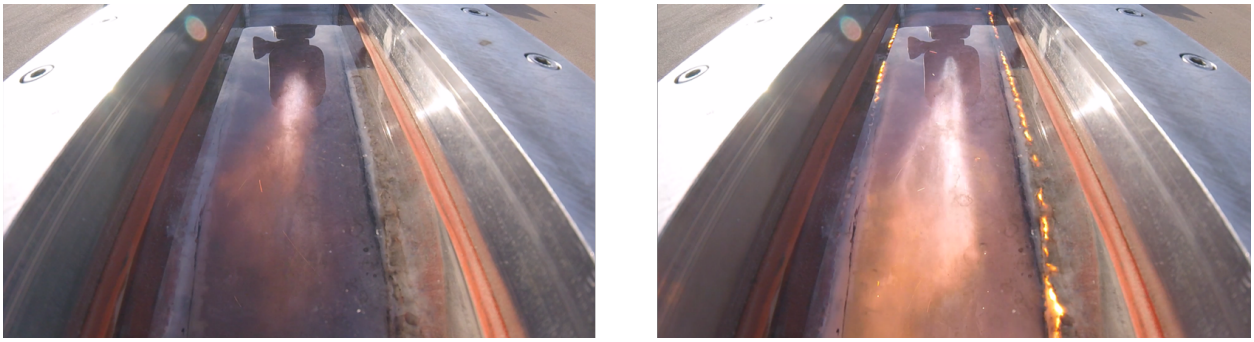

Figure 12. The main burner ignition at two different times for Case 1

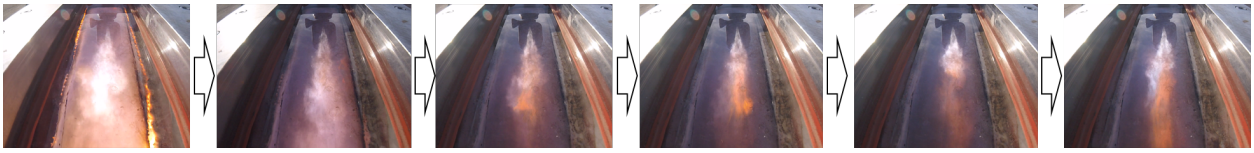

Figure 13. Main burner firing for Case 1 (7 bar) and 160kW power input

The volumetric flowrates for the igniter methane, igniter oxygen, main burner methane and main burner oxygen is shown in Fig. 14 (left). The O/F ratio during the igniter operation is close to 2, which is fuel rich. From Fig. 13 it can be seen that the flame is yellow in color, characteristic of a fuel rich environment. The corresponding pressure curve for the experiment is seen in Fig. 14 (right).

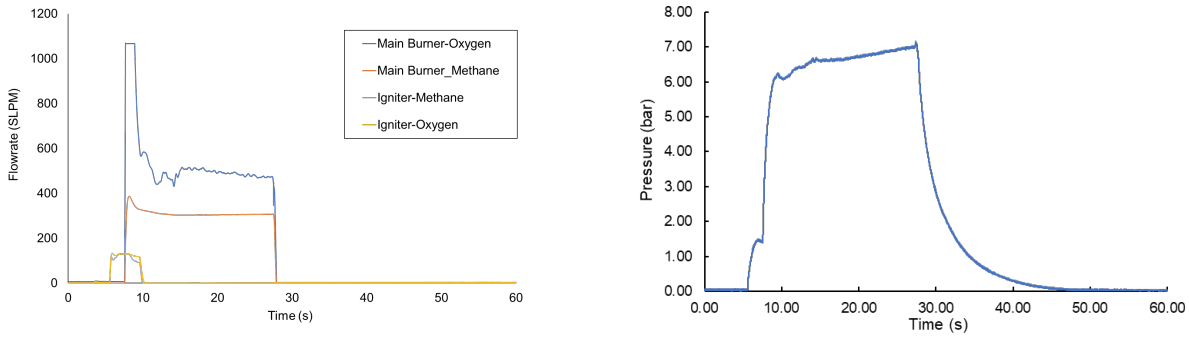

Figure 14 Case-1 - (Left) Volumetric flowrate of fuel and oxygen and (Right) Combustor pressure during the case 1 experiment

Figure 14 (right) shows that the chamber pressure initially rises up to 2 bar as the igniter is initiated. The flow through the main burner is then initiated after 2s of igniter operation. Thus, there are 2s of overlapping operation between the main burner and the igniter. The oxygen volumetric flowrate initially spikes up to 1100 standard liters per minute (SLPM) and gradually decreases to 500 SLPM. Figure 13 shows the flame from the primary burner during the test. The O/F ratio during the main burner operation is 3.3. Qualitative observation of the flame shows that it is highly turbulent and has the initiation of a wrinkled flame front. The chamber pressure during the operation raises up to 7 bar.

During the experiment the burner was tested up to a 16 bar pressure (case 2) and operating at a power rating of 220 kW. The main burner is operated for 30s for case 2. Figure 15 shows the volumetric flowrate, pressure and temperature data for this case. It is found that for both cases there are significant oscillations in oxygen flowrate. This may occur due to the flowmeter. Figure 14 (b) shows the pressure profile during the test. It can be seen that the chamber pressure goes up to 8 bar as soon as the main briner is initiated. Afterwards the chamber pressure gradually increases to 16 bar.

A thermocouple is inserted into the combustion chamber to measure the near wall gas temperature. The thermocouple probe is situated 438 mm away from the combustor inlet. Figure 15 (c) shows the near wall gas temperature inside the combustor. It can be observed that the near wall gas temperature reaches 1400 K, which is close to the melting point of stainless steel. A cooling system must be introduced for steady state operation. The CFD analysis for case 2 is ongoing based on results obtained from case 1.

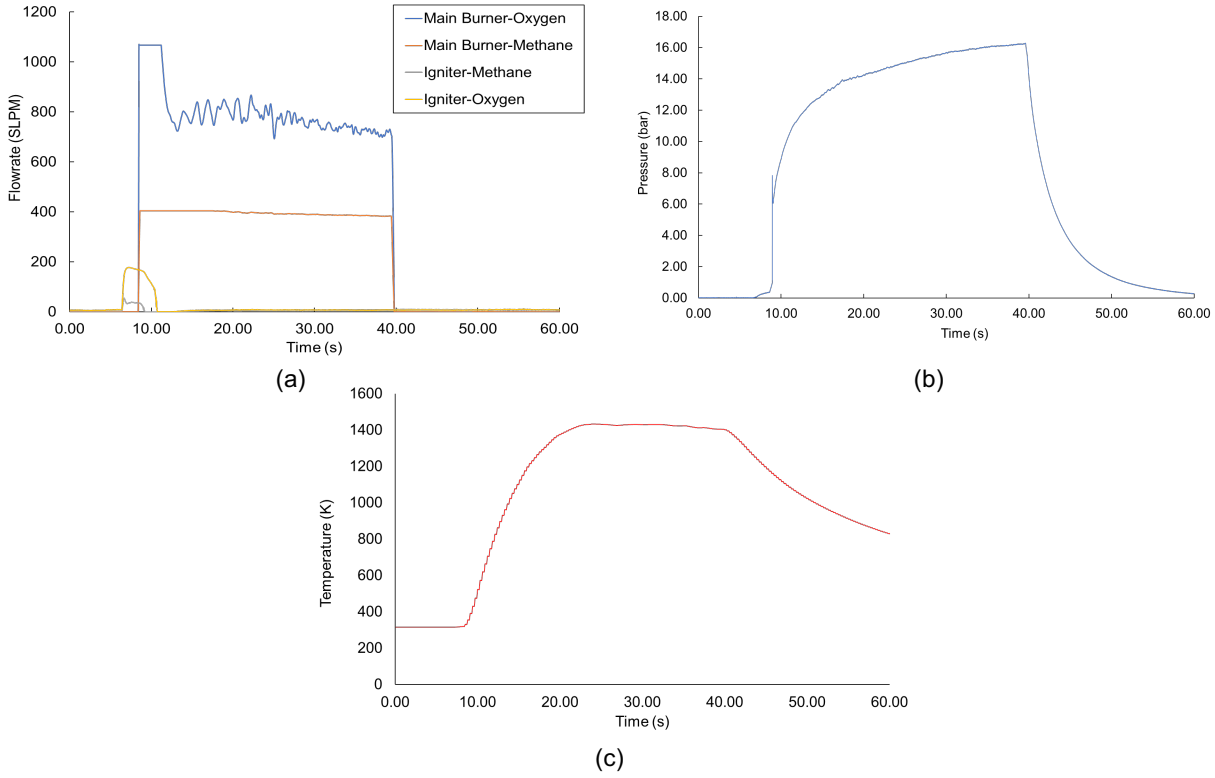

Figure 15 Case-2 (a) Volumetric flowrate of fuel and oxidizer, (b) Pressure inside combustor, and (c) Wall-temperature during the experiment

A qualitative and quantitative comparison is made between the CFD model and the experimental results. During the CFD analysis the C_P value of the combustion products was modified to take into account the disassociation of the reaction. The adiabatic flame temperature for oxygen gas mixtures reach extremely high temperatures (>2500K). Under these conditions, the equilibrium disassociation of the reaction products must be considered for CFD. The combustion temperature profile from the CFD without CO_2 dilution can be seen in Fig. 16. It is observed that the maximum flame temperature reaches 3135 K. For the same case, the adiabatic flame temperature was calculated to be 3300 K from NASA CEA for the same fuel and oxidizer mixture ratio without

dilution. The O/F mixture ratio for the NASA CEA case is 3.3. The difference between the flame temperature obtained from NASA CEA and CFD analysis is 5%. Figure 17 (a-b) presents the temperature and pressure profiles at different times in the CFD analysis.

For the model with the same inlet conditions, the chamber pressure reaches 11 bar while experiments reached 7 bar. A 100 fold rise in temperature compared to the experiment is also observed. Temperature rises to 1800 K in 80 milliseconds. Factors that may contribute to discrepancies in the temperature and pressures include leakage in the actual combustor, heat losses to the walls, valve response times, combustor fill volume, and flow restrictions which are not considered in the model. Secondary effects such as inaccuracies in the prediction of product gases due to the simplified one-step model may result in inaccuracies in the specific heat values of the gas.

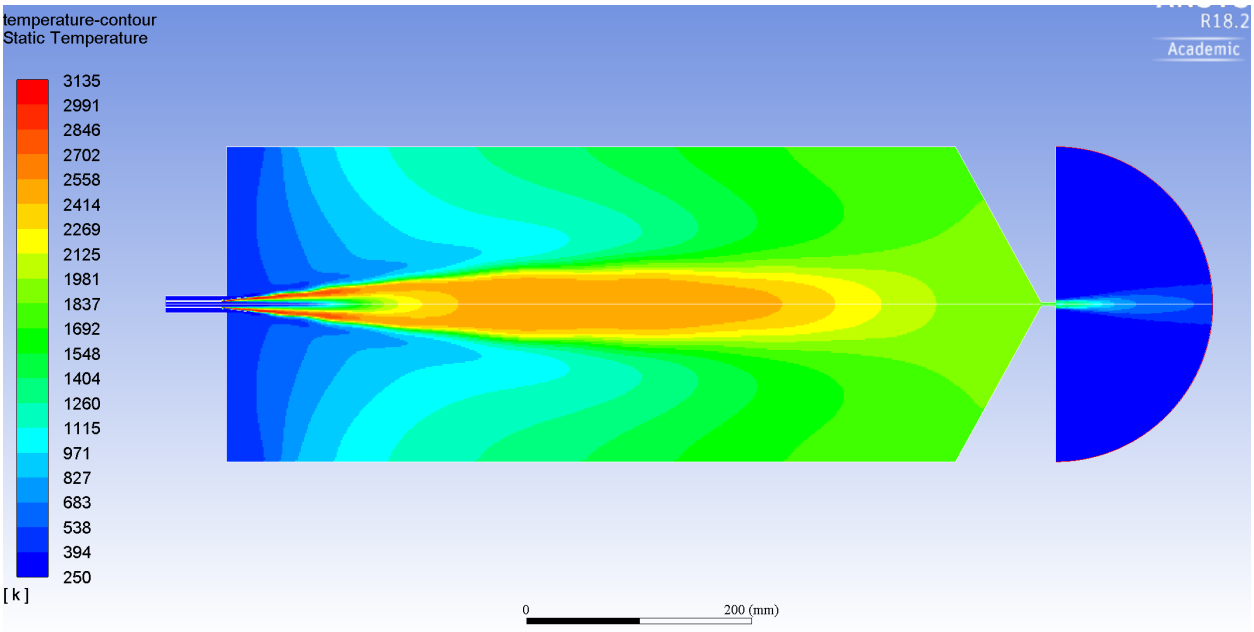

Figure 16 Case-1 – Model results for temperature profile inside the combustor

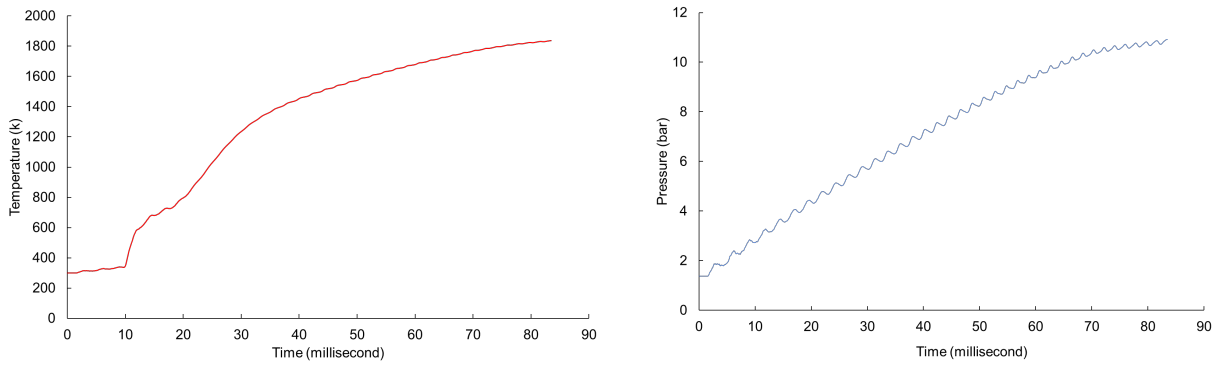

(a) (b)

Figure 17. Case-1 modeling results for (a) Wall temperature and (b) Chamber pressure.

SUMMARY AND CONCLUSIONS

The purpose of this experimental study is to systematically develop needed tools for supercritical combustion systems. Hence, the design and testing of a combustor that can operate at up to a 250 kW power input and 20 bar pressure is presented. Although 20-bar does not represent a supercritical test condition, it is an intermediate step that is immediately experimentally achievable.

Data obtained from this study including system start-up, ignition, and steady operation is useful for ongoing modeling efforts. For this study, test data is acquired for two cases: 160 kW firing input at a 7 bar chamber pressure (case 1) and 220 kW firing input and 16 bar chamber pressure (case 2). CFD analysis is performed to simulate the combustion process for case 1.
The simulation is conducted using a 2D domain. The CFD results match with NASA CEA within 5% without CO_2 dilution. In the CFD model, a 100 fold rise in temperature compared to the experiment is also observed. Temperature rises to 1800 K in 80 milliseconds. Factors that may contribute to discrepancies in the temperature and pressures include leakage in the actual combustor, heat losses to the walls, valve response times, combustor fill volume, and flow restrictions which are not considered in the model. Secondary effects such as inaccuracies in the prediction of product gases due to the simplified one-step model may result in inaccuracies in the specific heat values of the gas. Furthermore, in order to validate the CFD modeling approach it is likely that more detailed experimental data such as temperature profiles, CO exhaust measurements, and other combustion parameters are needed.

REFERENCES

[1]Glarborg, P., & Bentzen, L. L., "Chemical effects of a high CO2 concentration in oxy-fuel combustion of methane," Energy & Fuels, Vol. 22, No. 1, 2008, pp. 291-296.
[2]Zhang, N., & Lior, N., "Two novel oxy-fuel power cycles integrated with natural gas reforming and CO2 capture," Energy, Vol. 33, No. 2, 2008, pp. 340-351.
[3]Buhre, B. J. P., Elliott, L., Sheng, C. D., Gupta, R. P., & Wall, T. F., "Oxy-fuel combustion technology for coal-fired power generation," Progress in energy and combustion science, Vol. 31, No. 4, 2005, pp. 283-307.
[4]Stadler, H., Beggel, F., Habermehl, M., Persigehl, B., Kneer, R., Modigell, M., & Jeschke, P., "Oxyfuel coal combustion by efficient integration of oxygen transport membranes," International Journal of Greenhouse Gas Control, Vol. 5, No. 1, 2011, pp. 7-15.
[5]Hong, J., Chaudhry, G., Brisson, J. G., Field, R., Gazzino, M., and Ghoniem, A. F., "Analysis of oxy-fuel combustion power cycle utilizing a pressurized coal combustor," Energy, Vol. 34, No. 9, 2009, pp. 1332-1340.
[6]Liu, C. Y., Chen, G., Sipöcz, N., Assadi, M., & Bai, X. S., "Characteristics of oxy-fuel combustion in gas turbines," Applied Energy, Vol. 89, No. 1, 2011, pp. 387-394.
[7]Matuszewski, M., "Advancing oxycombustion technology for bituminous coal power plants: an R&D guide," US Department of Energy Final Report, 2010/1405, April 2012.
[8]Carroni, R., Griffin, T., Mantzaras, J., & Reinke, M. (2003). High-pressure experiments and modeling of methane/air catalytic combustion for power-generation applications. Catalysis Today, 83(1), pp. 157-170.
[9]Stephen, D. T., Zhu, D., & Law, C. K. (2004). Optically accessible high-pressure combustion apparatus. Review of scientific instruments, 75(1), pp. 233-239.
[10]Singla, G., Scouflaire, P., Rolon, C., & Candel, S. (2005). Transcritical oxygen/transcritical or supercritical methane combustion. Proceedings of the combustion institute, 30(2), pp. 2921-2928.
[11]Karataş, A. E., & Gülder, Ö. L. (2012). Soot formation in high pressure laminar diffusion flames.

Progress in Energy and Combustion Science,38(6), pp. 818-845.
[12]Sarker, S., Nunez, J., Valdez, C., Hossain, S., Love, N., & Choudhuri, A., "Preliminary design of an optically accessible high-pressure combustor," Proceedings of the Institution of Mechanical Engineers, Part C: Journal of Mechanical Engineering Science, Vol. 229, No. 3, 2015, pp. 505-517.
[13]Lux, J., & Haidn, O., "Effect of recess in high-pressure liquid oxygen/methane coaxial injection and combustion," Journal of Propulsion and Power, Vol. 25, No. 1, 2009, pp. 24-32.
[14]Ahmed, S., & Krumpelt, M., "Hydrogen from hydrocarbon fuels for fuel cells," International journal of hydrogen energy, Vol. 26, No. 4, 2001, pp. 291-301.
[15]Bromberg, L., Cohn, D. R., Rabinovich, A., O'Brie, C., & Hochgreb, S., "Plasma reforming of methane," Energy & fuels, Vol. 12, No. 1, 1998, pp. 11-18.
[16]Kendrick, D., Herding, G., Scouflaire, P., Rolon, C., & Candel, S., "Effects of a recess on cryogenic flame stabilization," Combustion and Flame, Vol. 118, No. 3, 1999, pp. 327-339.
[17]Tripathi, A., Juniper, M., Scouflaire, P., Rolon, J. C., Durox, D., & Candel, S. (1999, June). "LOx tube recess in cryogenic flames investigated using OH and H2O emission," 35th Joint Propulsion Conference and Exhibit, California, 1999,p. 2490.
[18]Wheeler, D. B., & Kirby, F. M., "High-pressure LOX/CH4 injector program," NASA Report, 1979.
[19]Sanchez, L. E., Chaparro, J., Torres, S. A., Love, N. D., & Choudhuri, A. R. (2016). "Development and Testing of a O2/CH4 Torch Igniter for Propulsion Systems," 52nd AIAA/SAE/ASEE Joint Propulsion Conference, Utah, 2016, pp. 4975.
[20]Cengel, Y. A. (2010). Fluid mechanics. Tata McGraw-Hill Education.
[21]de la Torre, M., Chowdhury, A. A., Love, N., & Choudhuri, A. (2016). Radiative heat release from premixed oxy-syngas and oxy-methane flames. Fuel, 166, 567-573.

ACKNOWLEDGEMENTS

This research is supported by the US Department of Energy, under award DoE Award Number: DE-FE-0029113 (Program Manager: Parrish Galusky) and Air Liquide. However, any opinions, findings, conclusions, or recommendations expressed herein are those of the authors and do not necessarily reflect the view of the Department of Energy and Air Liquide.